The International Journal of Advanced Manufacturing Technology (2024) 131:483–504
https://doi.org/10.1007/s00170-024-13039-3

ORIGINAL ARTICLE

Numerical parameter sensitivity analysis of residual stresses induced by deep rolling for a 34CrNiMo6 steel railway axle

Tobias Pertoll[1] · **Christian Buzzi**[1] · **Martin Leitner**[1] · **László Boronkai**[2]

Received: 31 July 2023 / Accepted: 13 January 2024 / Published online: 2 February 2024

Abstract

To optimise the benefits of the deep-rolling process in the service life context of treated components, the process application must be investigated. In addition to the reduction in surface roughness and near-surface material strengthening, compressive residual stresses are introduced, which are primarily responsible for the increase in service life for components, especially in the case of high-strength steel materials. A numerical parameter sensitivity analysis is performed in order to investigate the introduced residual stresses in detail. For this purpose, a validated deep-rolling simulation model is used, which replicates the deep rolling of a railway axle made of the high-strength steel material 34CrNiMo6. The model is based on an elastic-plastic Chaboche material model parameterised on uniaxial tensile and LCF test results and validated with residual stress measurements. Using this model as a basis, the effect of the main process parameters deep-rolling force, feed rate, friction coefficient, number of overruns, tool geometry, and shaft geometry on the resulting residual stress state are investigated. The results reveal that the deep-rolling force has the most significant influence on the introduced residual stress state and should therefore be highlighted. In the case of applying a deep-rolling force of more than 10 kN, maximum compressive residual stresses of around − 1000 MPa are introduced, and a strong saturating behaviour is shown. Maximum compensating tensile residual stresses of + 100 MPa occur below the surface. The main influence of the deep-rolling force is the effective depth achieved, which is determined by the depth of the zero crossing. This varies from 1 mm with an applied force of 2 kN to more than 3.5 mm with 20 kN. Furthermore, the results are analysed to conclude suggestions for the process's applicability, and a proposal for an optimised deep-rolling treatment is presented. There multiple deep rolling with decreased deep-rolling forces is used to achieve a comparably optimised residual stress state. In summary, with the presented results, a contribution to a deeper understanding of the deep-rolling process can be achieved; the influence of the most important process parameters on the residual stress in-depth profiles is established; an optimisation proposal is presented; and correlations are found. Thus, the base work for further fatigue strength assessments and the optimisation of the deep-rolling process regarding the increase of service is laid.

Keywords Mechanical surface treatment · Deep (cold) rolling · Railway axle · 34CrNiMo6 · Residual stress · Finite element method · Parameter sensitivity analysis

1 Introduction

Mechanical surface post-treatments are often used as strengthening treatments because of their simple, economical, and efficient application. Their application improves the surface properties, and as a result, the component service life can be increased, or, on the other hand, the component weight can be reduced while simultaneously retaining the service lifetime. Furthermore, post-treatments have a significant influence on crack initiation and crack propagation [1, 2]. On the mechanical surface, post-treatment processes include shot peening [3, 4], burnishing [5, 6],

✉ Tobias Pertoll
tobias.pertoll@tugraz.at

[1] Institute of Structural Durability and Railway Technology, Graz University of Technology, Inffeldgasse 25/D, 8010 Graz, Austria

[2] Siemens Mobility Austria GmbH, Eggenberger Strasse 31, 8020 Graz, Austria

deep rolling [7, 8], and also treatments like high-frequency mechanical impact post-treatment (HFMI) [9, 10]. These very different processes have different advantages, such as surface quality, achieved depth effect, and accessibility, among others. As a result, they are used in different industrial sectors. In this publication, the focus is laid on the investigation of the deep-rolling process. This process is used in automotive, aerospace, power generation, medical applications, and also in railway applications. Thereby, the process is mainly applied for the post-treatment of railway axles because it is very effective, has a deep penetrating effect, and is therefore well suited for such large components [8, 11, 12].

Deep rolling is one of the few post-treatment processes that achieves three life-enhancing effects with one process application. The surface roughness is reduced, the near-surface region is strengthened, and compressive residual stresses are introduced [7]. The potential for increasing service life strongly depends on the treated material. While a lower surface roughness is generally considered to increase the service life, strain hardening has a life-increasing effect, especially for materials with low-yield strength and high-strength titanium alloys. For materials with a high yield strength, the introduced residual stresses are particularly important [13, 14]. Several studies on the deep-rolling process can be found in the literature. However, because of the strong material dependence of the process effect, a distinction must be made. Although there are studies on aluminium alloys [15, 16], titanium alloys [17, 18], magnesium alloys [19], and various types of steel, including stainless steel [20–22], only a few publications have so far focussed on high-strength steels [23, 24].

In addition to the steel materials EA1N and EA4T, which are considered in the European Railway standard for the design of railway axles [25], the high-strength steel 34CrNiMo6 is used for the application of railway axles [26–28]. This research work investigates the application of the deep-rolling process on railway axles made of this material.

The deep-rolling process is mainly used for rotationally symmetrical components. A deep-rolling tool, usually a hydrostatically beared ball tool or, as in this case, a mechanically beared disc tool [29], is pressed onto the rotating component and displaced in the longitudinal direction with a defined feed rate. The surface is treated helically as a result. In the contact between the tool and the component, the material plasticises, and thus the aforementioned positive effects are achieved. The introduced residual stress depth profile typically appears as described in the following: In the surface near the region, residual compressive stresses are introduced, with their maximum occurring at or slightly below the surface. Underneath, the residual compressive stresses reduce and, after zero crossing, change to a compensating tensile residual stress range [30].

In the design standards and guidelines for cyclically loaded components, such as the FKM guideline [31] and DIN 743 [32], the benefits of applying mechanical post-treatment processes are only permitted in a limited form. No benefit may be considered for railway axles since the standards do not consider any service life benefit for larger shaft diameters. New approaches such as “Estimation of the fatigue strength of edge-strengthened components” in the Appendix of the FKM go a step further and take the process application into account. To fully exploit the benefits, the hardening depth profile and the residual stress depth profile must be known. While the hardness depth curve is easy to determine by measurement, the residual stress depth curve is more difficult to establish. The residual stress depth curve in the near-surface area can be well measured using the common measuring methods of hole drilling (HD) and X-ray diffraction (XRD). Measuring at greater depths is more difficult. The measurement depth of the HD method is limited because of the process itself, and the XRD approach uses electrochemical removal between the measurement points, which results in a modification of the zero crossing and a reduction of the tensile residual stress range. To remedy this problem, a detailed numerical model of the deep-rolling process has been developed and presented in [33]. By considering the electrochemical removal, the simulation model is validated with residual stress measurements to ensure its proper simulation results.

The simulation model consists of several deep-rolling tools and a representative flat model that is deep-rolled. The difficulty in simulating the deep-rolling process is the multiple occurring non-linearities contact, material model, and the large deformations that occur. An elastic-plastic Chaboche material model is therefore assigned to the flat simulation model to be able to correctly represent the introduced residual stresses. The model is parameterised on the basis of the results of tensile and low-cycle fatigue (LCF) tests carried out on specimens taken from the surface layer of a railway axle. The model is briefly presented in the following chapter, whereas further details are provided in [33]. However, this publication primarily focuses on the investigation of the influence of different parameters on the introduced residual stress in-depth profiles. Therefore, a reference model is defined based on the validated simulation model, and the influence of the most important deep-rolling parameter is investigated. Such a sensitivity analysis is important to determine the influence of the parameters so that the residual stress depth curve can be further optimised in the component service life context.

In [12], the parameters that influence the result of the application of the deep-rolling process are listed and classified as shown in Fig. 1. The classification of the parameters is conducted into workpiece, tool, process, and device. In green and red, the influences are marked, which can be

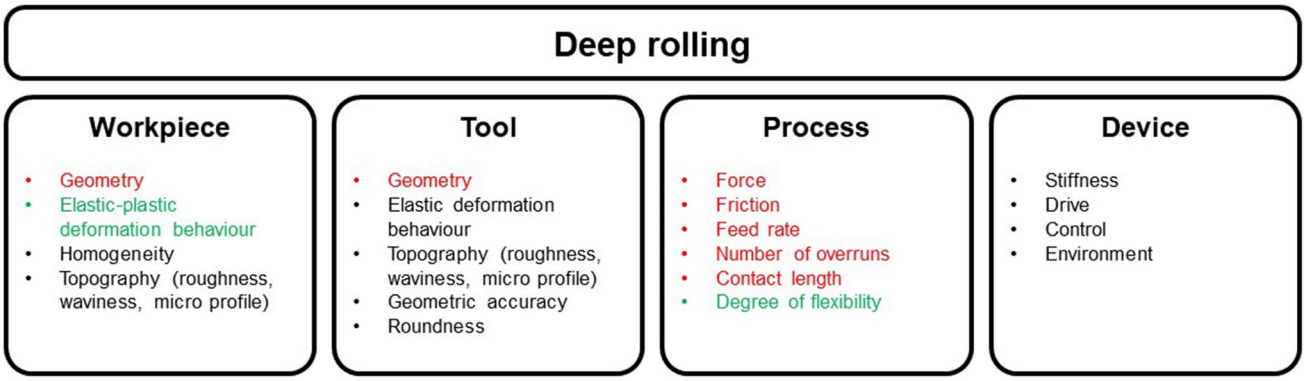

Fig. 1 Influencing parameters with an impact on the deep-rolling process application result [12]. Marked considered parameters in the FE simulation (red and green) and investigated parameters in this publication (red)

investigated using the presented finite element simulation model of the deep-rolling process. However, in the investigation presented, the main focus is on the essential parameters, marked red in Fig. 1. The influence of the force, the feed rate, the friction, the number of overruns, the tool geometry, here the tool diameter and the contact radius, and the simulation model geometry, in this application case the shaft geometry, are investigated. The contact length is not considered as an explicit parameter; it is indirectly observed through the changed geometries. The scope of this work is limited to the steel material 34CrNiMo6. The degree of flexibility in the process section is limited by the use of disk tools and the deep rolling of rotationally symmetrical components. Investigation in the context of parameter variation is thus not relevant.

Studies into the effect of deep-rolling parameters on the residual stresses introduced are limited. As the influence of the process application is strongly material-dependent, it can be assumed that the parameter influence is also material-dependent and must therefore be explicitly investigated for the material used. Nevertheless, some important studies should be mentioned in which the results of the different parameters are presented. However, no guarantee of completeness can be given. Table 1 provides an overview of the existing literature, considering experimental and simulation parameter sensitivity studies. The investigations are divided into material groups in the table. They are divided into titanium, aluminium, steel, magnesium, and brass alloys. Some publications with deep-rolling parameter variations on steel materials were found, but again, only very few references on higher-strength steel materials can be found [34]. In the literature, variations of the parameters force, feed, friction, tool geometry, multiple overruns, and rolling speed have been noticed. The most frequently investigated parameters, both with simulations and experiments, are the deep-rolling force and the influence of the feed rate. Investigations on the coefficient of friction, multiple deep rolling, tool geometry, and different shaft geometries were rarely or not at all investigated. Friction has, so far, only been investigated in a simulative way. Experimental and simulative results were found in the literature for the investigation of multiple deep rolling, tool geometry, and rolling speed parameter studies.

Apart from the rolling speed, which cannot be adequately simulated by applying the given finite element model with a strain rate-independent material behaviour, the influence of all other parameters found in the literature, as well as the influence of the geometry of the simulation model, in this case, shaft geometry, are presented in the following sections.

Therefore, the scientific contribution of this research work can be highlighted as follows:

- A comprehensive numerical deep-rolling parameter study considering all essential deep-rolling parameters for deep rolling of railway axles
- An extensive enhancement of the influence on the introduced residual stresses for the material group steel alloy
- A representation of the residual stress in-depth curves in circumferential and longitudinal directions whereby each parameter influence is examined exclusively and discussed
- An evaluation of the parameter influence on the characteristic residual stress in-depth parameters and presentation of the found correlations
- An overview and evaluation of the impact of deep-rolling parameters on the introduced residual stresses in terms of process applicability
- A presentation of a novel deep-rolling process optimisation proposal

Table 1 Evaluation of the existing literature on the influence of the experimental (E) and simulation (S) deep-rolling and burnishing parameter variations on the introduced residual stresses

	Force/pressure	Feed rate/ overlap	Friction	Tool geometry	Multiple over-runs	Rolling speed
Steel alloy						
Hassani-Gangaraj et al. [11]	S	S		S		
Lyubenova et al. [35]	S	S			S	
Alshareef et al. [36]	E	E				E
El-Axir [37]	E					E
John et al. [6]	E/S	E/S				E/S
Sartkulvanich et al. [34]	S	S				
Rami et al. [38]	E	E		E		E
Majzoobi et al. [39]	S	S		S		S
Titanium alloy						
Bäcker et al. [40]	E/S	E/S		E/S		
Klocke et al. [41]	E/S					
Han et al. [42]	E/S	E/S	S	E/S	E/S	E
Lim et al. [43]			S			
Manouchehrifar et al. [44]	S	S	S			
Mohammadi et al. [45]	S	S		S	S	
Hadadian et al. [30]		S				
Sayahi et al. [46]	E/S			E/S		
Aluminium alloy						
Beghini et al. [15]	E	E				
Magnesium alloy						
Uddin et al. [19]	S	S				
Brass alloy						
Mombeini et al. [47]	S	S	S	S	S	

2 Methodology

2.1 Reference deep-rolling simulation model

In this publication, the influence of the most important deep-rolling parameters, marked in red in Fig. 1 on the in-depth residual stress profile is numerically investigated. The simulation model is presented in [33], which acts as a basis for this parameter study. In the following, an overview of the model is given, whereas further details are provided in [33]. The model is built in the commercial finite element simulation software MSC Marc. It is an implicit 3D simulation model that replicates the deep-rolling process applied to a railway axle, visible in Fig. 2 (left). It consists of deep-rolling tools and a representative flat model, whereas the transferability to real railway axle geometries is ensured; see [33]. Between the tools and the model, a contact exhibiting a friction coefficient of $\mu = 0.1$ is defined. The deep-rolling tools are disc shapes, which are modelled as analytically described rigid bodies, equalling a good assumption due to the significantly higher stiffness of the used tools. The simulation model is meshed with 8-node linear hexahedral elements with a linear shape function. The direction X (rolling direction) corresponds to the circumferential direction of the railway axle, the direction Y (feed rate direction) to the longitudinal direction, and the Z-direction to the radial direction, defined positively from the surface to the inner. The size of the representative flat model and the mesh size are determined by sensitivity analyses. Except for the contact surface, on all sides of the model, symmetry constraints are defined to represent the surrounding material. The tools are arranged in parallel in the start position in the simulation. The distance between them corresponds to the feed rate of the process application. The tools roll over the representative flat model one after the other. This represents the reality in which, after one turn of the railway axle, the deep-rolling tool reaches the same position as it has just been displaced in the longitudinal direction by the applied feed. The delay between the tools is defined in such a way that the tools do not influence each other and thus have no impact on the residual stress generation. Each tool is controlled by a central node. In the first step, the deep-rolling force is applied to this node of the first tool. When the force is fully applied, the tool is

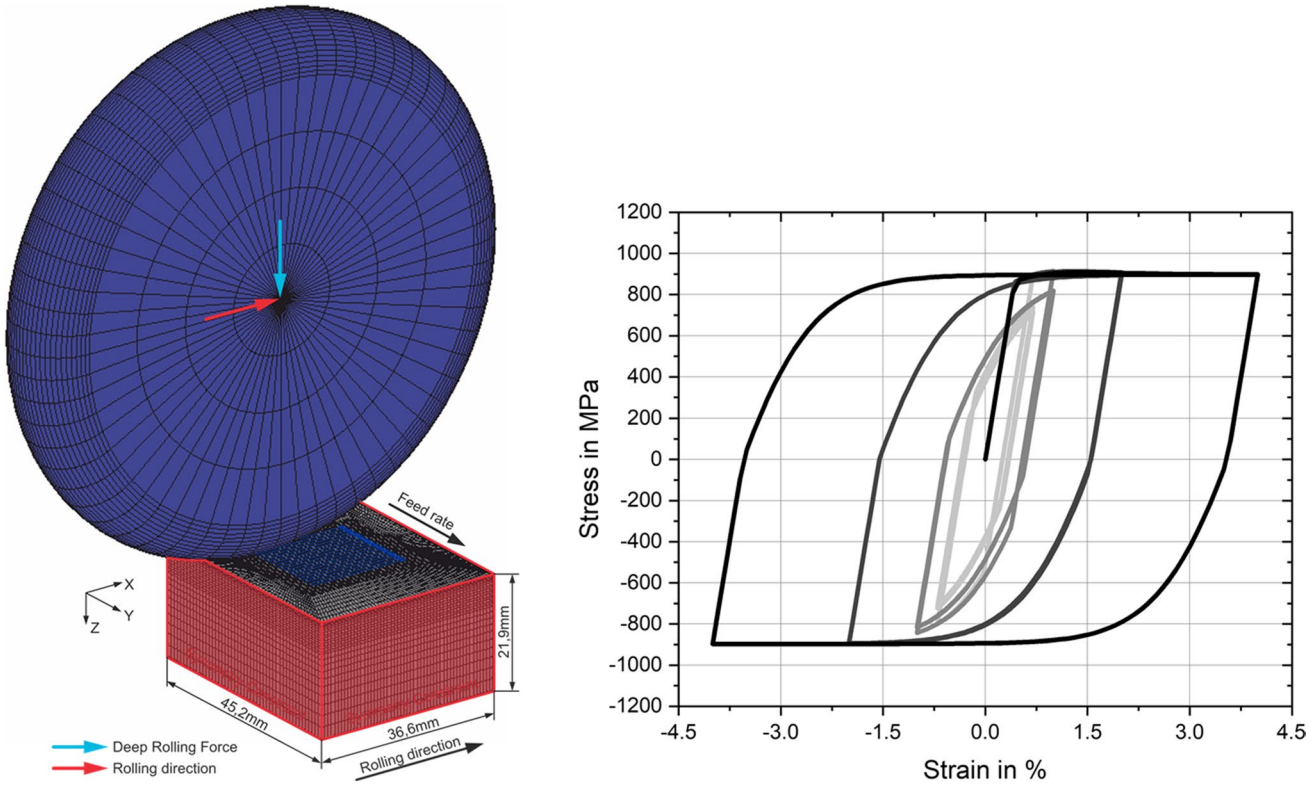

Fig. 2 Deep-rolling simulation model (left) and parameterised Chaboche material model response to several applied strains (right)

displaced in the rolling direction. Due to the friction contact, the tool rolls over the surface, and finally, the force is reduced again. This procedure is repeated for all tools.

An elastic-plastic material model is assigned to the workpiece in order to properly evaluate residual stresses. The material used is a high-strength steel 34CrNiMo6. To determine the material characteristics, uniaxial tensile tests and cyclic tests are carried out on specimens extracted from the surface layer of a non-deep-rolled section of a railway axle. Based on these test results, the Chaboche material model implemented in MSC Marc is parameterised, visible in Fig. 2 (right). Details of the material model are again given in [33].

The deep-rolling parameters of the reference simulation model can be summarised as follows:

- Deep-rolling force: 20 kN
- Feed rate: 0.5 mm
- Friction coefficient: 0.1
- Number of overruns: 1
- Deep-rolling tool geometry
  - Diameter: 100 mm
  - Contact radius: 9 mm
- Simulation model/shaft geometry: flat/not considered

To verify the correct function of the model, it must be validated. Therefore, the residual stress in-depth profile, also considering the electrochemical removal process in the numerical simulation, is compared with residual stress measurements determined by XRD and HD methods. The comparison presented in [33] exhibits sound agreement revealing that the used simulation model is well capable of numerically assessing local residual stress conditions by the deep-rolling process.

Figure 3 (left) depicts the graphical simulation result with a quarter of the model hidden. The von Mises stresses are shown as a simulation result applying the afore-described reference model parameters. In the figure, the steady residual stress surface state in the middle and the surrounding transition zones to the constraints can be seen. Furthermore, the developing residual stresses in depth can be observed graphically. To determine the in-depth residual stress curves, the residual stresses are evaluated in the centre of the model along the marked path. These stress curves correspond to the prevailing stress state in the component. Figure 3 (right) shows the residual stress curves in the circumferential, longitudinal, and radial directions.

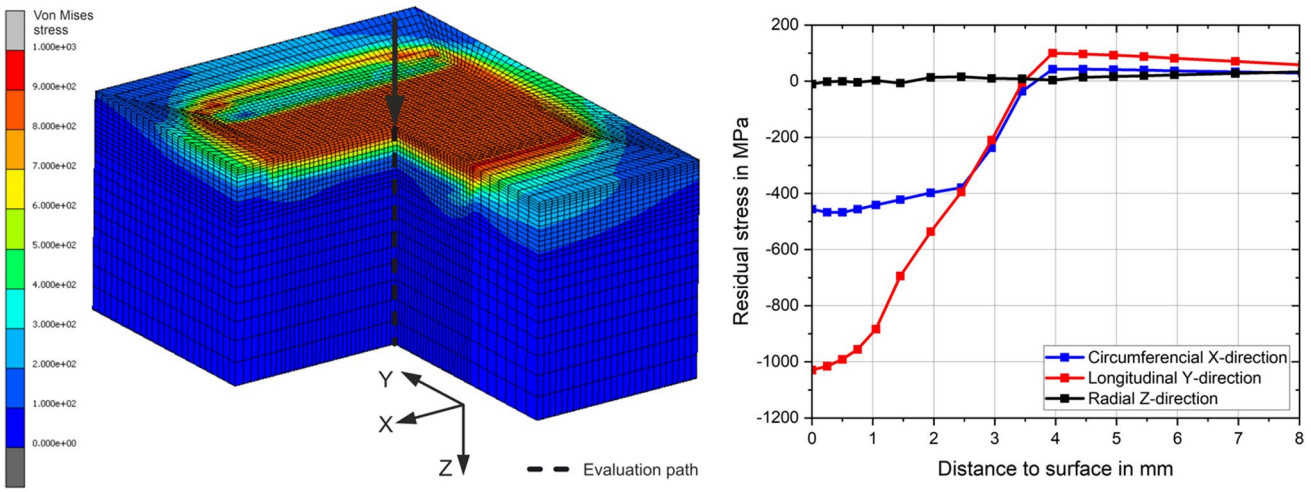

Fig. 3 Simulation result, visible are the von Mises stresses, with marked evaluation path (left) and the resulting residual stress in-depth distribution evaluated along the evaluation path (right)

2.2 Investigated deep-rolling parameter

As already mentioned, in this research, the influence of different deep-rolling parameters on the resulting residual stresses is investigated. For this, the presented reference model is used as a basis, individual parameters are changed, and the result is recalculated. Only one deep-rolling parameter is adjusted at a time to exclusively determine the influence of this parameter. Within the scope of the investigation, the influence of the deep-rolling force, the feed rate, the friction coefficient, the number of overruns, the tool geometry, and the shaft geometry are examined. The following subsections describe the changed parameters and how the parameters are changed in the simulation.

2.2.1 Deep-rolling force

The deep-rolling force is the force by means of which the tools are pressed onto the surface of the representative flat model to be treated during the deep-rolling process. The deep-rolling process is usually force-controlled, which means that the deep-rolling force is kept constant during the process application. In the simulation used for validation and also in the reference model, a deep-rolling force of 20 kN is applied. In addition to the 20 kN, simulations with 18, 15, 12, 10, 5, and 2 kN are conducted.

2.2.2 Feed rate

The real feed rate is reproduced in the simulation with several tools rolling one after the other and next to each other. To change the feed rate in the simulation, the distance between the tools is adjusted. In addition to the results already shown for the reference model of 0.5 mm, the feeds of 0.25, 1, and 2 mm are examined.

2.2.3 Friction coefficient

When a friction coefficient is defined between the tools and the discretised simulation model, the rolling of the tools over the surface is achieved. The friction coefficient that occurs in reality cannot be easily determined. Therefore, in the reference simulation model, a typical steel-on-steel friction coefficient of $\mu = 0.1$ is assumed. This ensures that the tools roll over the surface according to reality. To investigate the influence of the friction parameter on the introduced residual stresses, the friction coefficients 0.03 and 0.3 of the simulation are used, and their influence is investigated.

2.2.4 Number of overruns

To investigate the influence of the number of deep-rolling process overruns, the above-described simulation process is repeated several times. The reference model is used as a basis, the simulation result of the first overrun is loaded, and the simulation procedure is repeated identically in the same area. The evaluation of overrun 2 is made along the same evaluation path after completing the second simulation run. This procedure is repeated for a third overrun.

2.2.5 Deep-rolling tool geometry

Due to the large dimensions of railway axles, disc tools are used to deep-roll railway axles. Their dimensions can be defined by their diameter D and the contact radius CR. These dimensions are defined by the manufacturers of the

deep-rolling tools, and therefore, the dimensions are not freely selectable for the user. The main objective of this study is not to simulate specific applications but to determine the trends for the influence of the individual parameters. Therefore, the influence of the two tool geometry parameters on the applied residual stresses is investigated individually.

Diameter The diameter of the reference tool is 100 mm. In addition to this, the fictitious diameters of 50 and 150 mm are examined, as shown in Fig. 4.

Contact radius The contact radius of the reference tool measures 9 mm. In addition to this, the contact radii of 5 and 12 mm are investigated, as shown in Fig. 5.

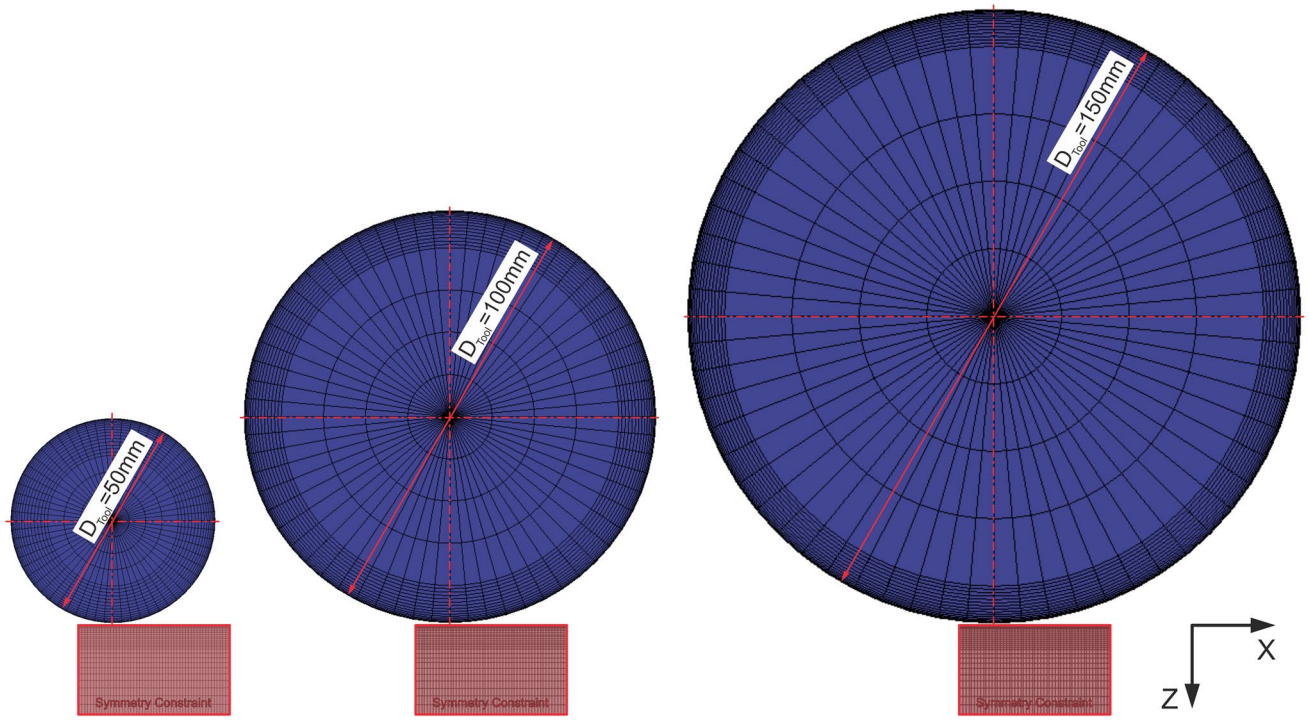

Fig. 4 Deep-rolling simulation models with different tool diameters. Tool diameter 50 mm (left), 100 mm (middle), and 150 mm (rig

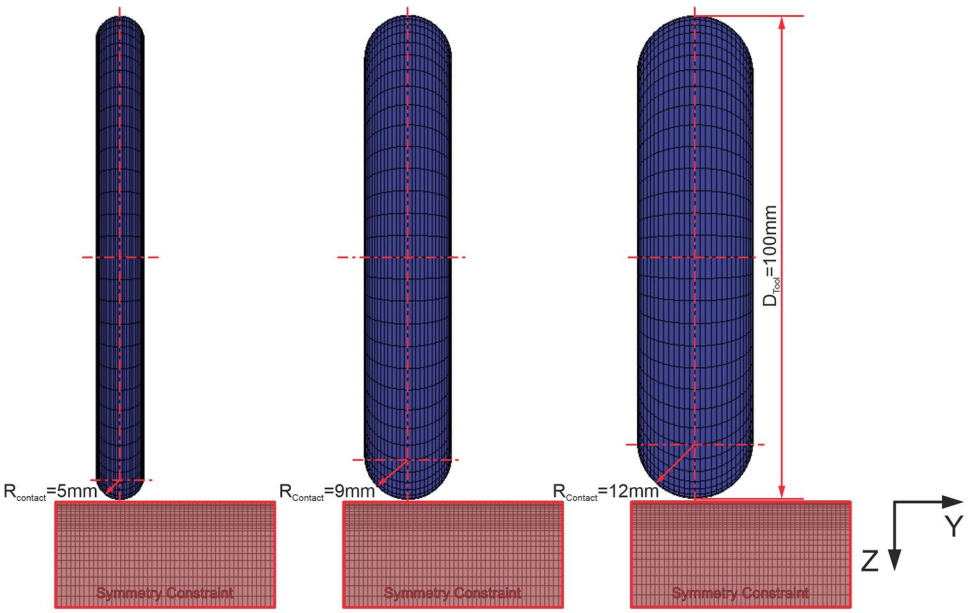

Fig. 5 Deep-rolling simulation models with different tool contact radii. Contact radius 5 mm (left), 9 mm (middle), and 12 mm (right)

2.2.6 Railway axle diameter

The previous investigations were carried out on the representative flat model. The simplified flat geometry reduces the modelling effort and results in a significantly shorter computation time. In [33], the validity and thus the transferability of the simulation result of the representative flat model to real railway axle applications are investigated with a simulation model with adapted outer railway axle geometry. The dimensions, the meshing, and the simulation procedure are identical or as similar as possible to the representative flat model. Details of the simulation model with the railway axle can be found in [33].

To investigate the influence of the railway axle diameter on the through-deep-rolling-introduced residual stress state, the simulation model with railway axle geometry must be used. Five simulation models with different railway axle diameters are built on the basis of this simulation model. The typical railway axle diameters of 114, 136, 158, 217, and 252 mm are investigated and shown in Fig. 6. Additionally, the representative flat model is considered a reference.

2.2.7 Process applicability and optimisation

A direct recommendation regarding the best choice of parameters is difficult just on the basis of the residual stresses introduced. Further detailed fatigue strength assessments and an investigation of the associated crack behaviour are necessary. Nevertheless, this section will attempt to provide recommendations for the application and present an optimisation proposal. Basically, it can be assumed that beneficial compressive residual stresses should prevail near the surface. The depth effect should be as deep as possible, and the suboptimal tensile residual stresses should be as low as possible. Multiple deep rolling with decreasing deep-rolling force shows optimised effects for these requirements and is presented in Section 3. Multiple deep rolling with 20 kN followed by 10 kN, with 20 kN followed by 5 kN, with 20 kN followed by 10 kN, and finally, with 5 kN, are compared in the study with the result of the reference simulation.

3 Results and discussion

In the following subsections, the influence of the investigated deep-rolling parameters presented in Section 2.2 on the introduced residual stresses near the surface is presented and discussed. The depth profile results are shown in the circumferential and longitudinal directions. In addition, the changes in the characteristic residual stress profile parameters are shown with respect to the investigated parameter. The following characteristic residual stress parameters of the depth profile are observed and can be seen in Fig. 7:

- The level (and depth) of maximal compressive residual stresses
- Depth of zero crossing (transition from compressive to tensile residual stresses)
- The level (and depth) of the maximal tensile residual stresses

To investigate in detail the influence of the deep-rolling parameters on the residual stresses, their influence is evaluated for all the investigated deep-rolling parameters on the three characteristic residual stress features mentioned. The shown points in the diagrams are the results of the evaluation of the simulations. In addition, the resulting relationship is approximated with suitable equations. Linear, quadratic, and exponential equations are used. The equations used and the corresponding parameters are indicated in the diagrams.

3.1 Deep-rolling force

Figure 8 shows the influence of the deep-rolling force on the residual stress depth curve in the circumferential (left) and longitudinal (right) directions. The deep-rolling force obviously has a significant influence on the induced residual stress state. Even the shape of the stress profiles changes fundamentally with low deep-rolling forces.

The influence of the deep-rolling force on the characteristic in-depth residual stress parameters, the maximum

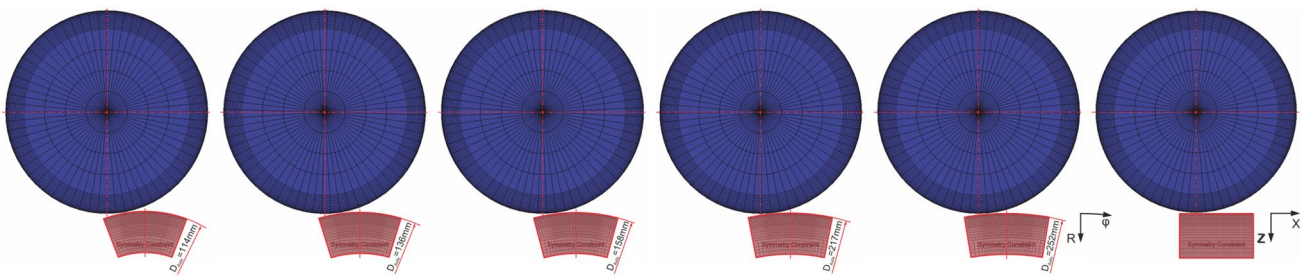

Fig. 6 Deep-rolling simulation models with different diameters of railway axles. Diameters from left to right are 114, 136, 158, 217, and 252 mm, and for comparison, additionally, the flat reference model is shown

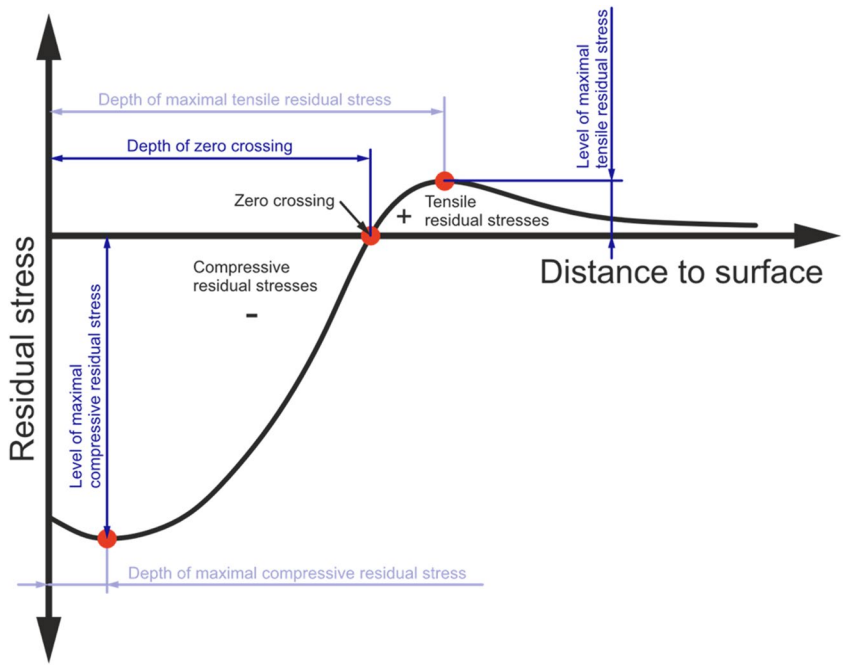

Fig. 7 Typical in-depth residual stress profile with marked characteristic residual stress parameters

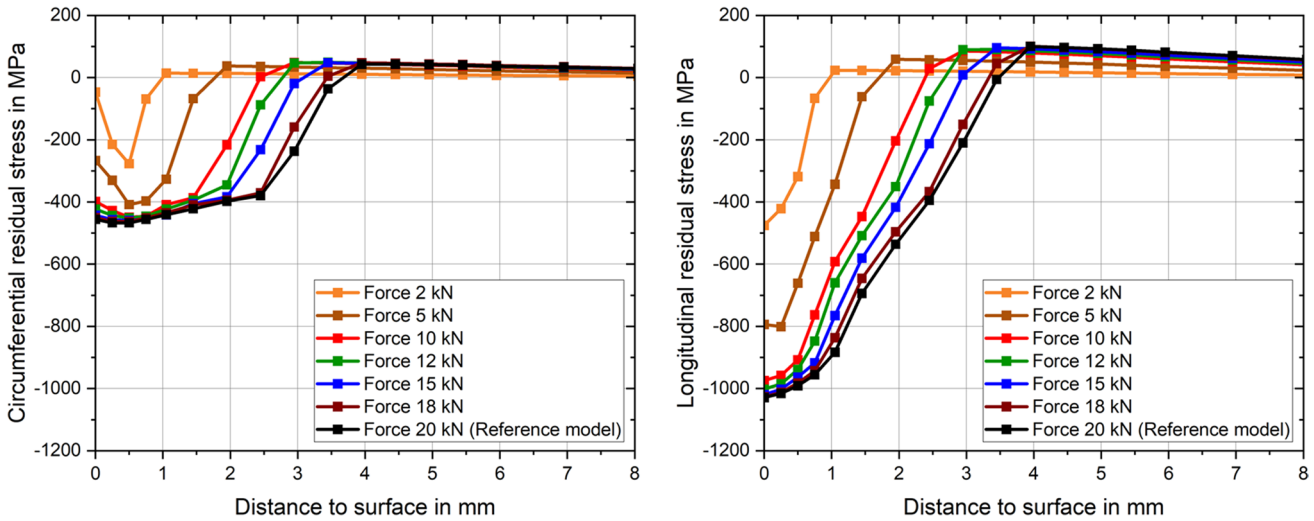

Fig. 8 Influence of the deep-rolling force on the residual stresses in the circumferential (left) and longitudinal (right) directions

compressive residual stresses introduced (left), the depth of the zero crossing (middle), and the maximum tensile residual stresses (right) are shown in Fig. 9. Higher deep-rolling forces result in more compressive residual stresses in the near-surface region. However, in the circumferential and longitudinal directions, a clear saturation behaviour with an approximation to a maximum value of around – 1000 MPa is evident. For deep-rolling forces below 10 kN, significantly lower maximum residual compressive stresses are introduced; above 10 kN, the differences are minor. The absolute value strongly depends on the material, the achievable maximum stresses of the material, and its representation in the material model.

The deep-rolling force has a significant influence on the depth of the resulting plasticisation, visible in the almost linear behaviour with a slightly flattening tendency towards higher forces. The deep-rolling force influences the achieved depth for the zero crossing. The major influence of the deep-rolling force on the depth of zero crossing and, thus, the effective depth of the process is an important parameter in the durability assessment of deep-rolled components.

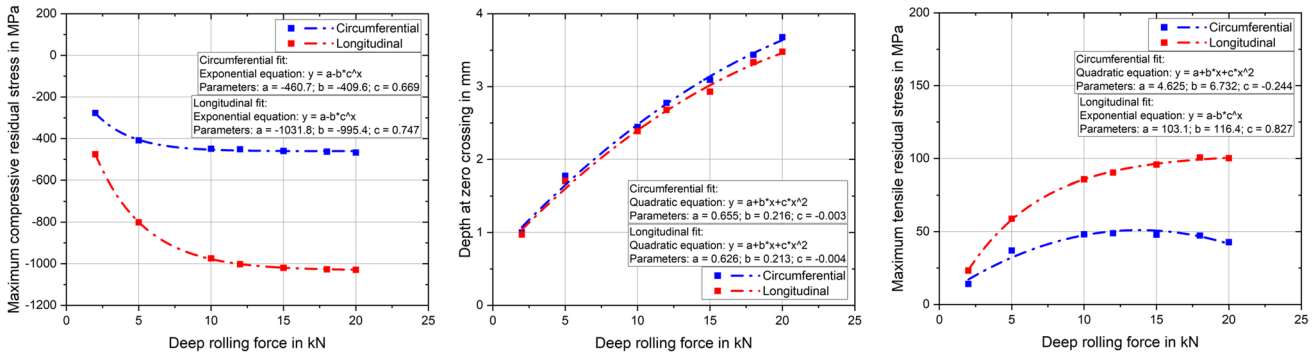

Fig. 9 Evaluation of the significant residual stress in-depth parameters versus deep-rolling force

The deep-rolling force also shows an influence on the maximum occurring compensating tensile residual stresses. In the longitudinal direction, the tensile residual stresses increase with increasing deep-rolling force, whereby saturation behaviour can also be seen here. In the circumferential direction, the behaviour is somewhat different. With small, deep-rolling forces, the tensile residual stresses increase until they reach a maximum of 10–15 kN. Above this, slightly reduced tensile residual stresses can be observed.

3.2 Feed rate

Figure 10 illustrates the influence of the feed rate on the residual stress depth curve. The feed rate of 0.5 mm was selected for the reference model to reduce the simulation time. As can be seen in Fig. 10, there is a negligible difference in the depth curve compared to the simulation result with a feed of 0.25 mm. The curves in the circumferential and longitudinal directions are almost congruent. A more pronounced difference can be seen in the curves resulting from the simulation with a feed rate of 1 and 2 mm, visible in Fig. 10. The feed shows an impact there, especially in the compressive residual stress range in the longitudinal direction.

The feed rate influences the homogeneity of the residual stress state. Figure 11 shows the graphical simulation results with 0.25, 0.5, 1.0, and 2.0 mm; visible are the von Mises stresses shown. Half of the model is hidden to show the distribution of residual stresses in-depth. At 0.25 and 0.5 mm, a very uniform residual stress region is formed, with 1.0 mm feed rate deviations already visible, and at 2.0 mm, an uneven residual stress state appears.

Figure 12 shows the effect of feed rate on the three defined significant characteristic values of the residual stress depth curves as a function of feed rate. The maximum compressive residual stresses in the circumferential direction do not change with different feed rates. In the longitudinal direction, where the change of the feed is realised with the distance between the tools, the maximum residual compressive stresses decrease with increasing feed rate. These differences can be related to the number of overruns at the same point. During the deep rolling with the deep-rolling force of 20 kN, the contact patch between the tool and the workpiece has a width of approximately 3 mm. This means for a feed rate of 0.5 mm, one point on the surface is directly treated by 7 tools and is in contact with even 7 tools one after the other. In addition, there are the tools beside that are not in

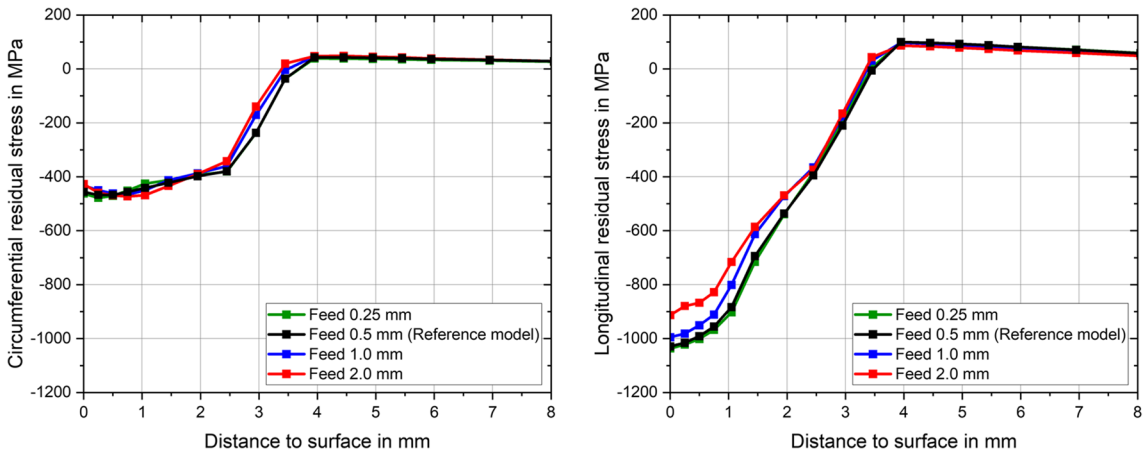

Fig. 10 Influence of the feed rate on the residual stresses in the circumferential (left) and longitudinal (right) directions

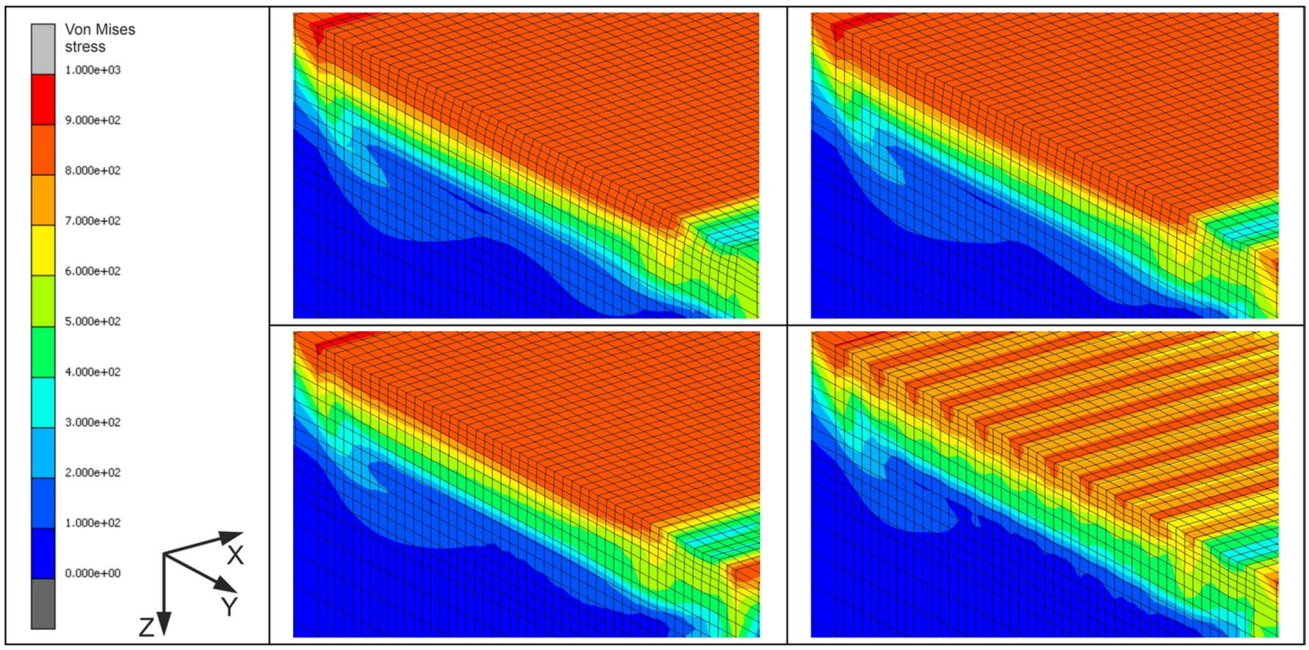

Fig. 11 Influence of the feed rate on the von Mises residual stresses. Feed rates of 0.25 mm (top left), 0.5 mm (top right), 1.0 mm (below left), and 2.0 mm (below right) are shown

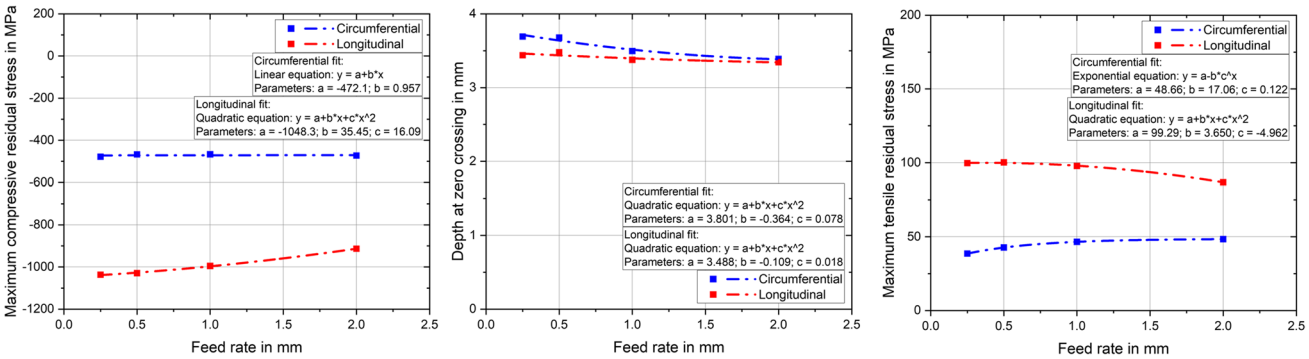

Fig. 12 Evaluation of the significant residual stress in-depth parameters versus feed rate

direct contact but whose load also has an influence on the point under consideration. The number of these treatments in the same range has a huge influence on the introduced accumulated plastic strain, and this further affects the material behaviour. The isotropic part of the used material model is dependent on the accumulated plastic strain and the resulting cyclic softening behaviour of the material. Therefore, the number of tools in contact at one point has an influence on the residual stress depth curve. In the reference model with a 0.5 mm feed, 7 tools come into direct contact; with a 0.25 mm feed, there are 13 tools; with a 1 mm feed, 4 tools; and with 2 mm feed, only 2 tools. The obvious major influence with 1 and 2 mm feed and the minor influence between 0.5 and 0.25 mm can be explained by the fact that at high feed, the saturation of the isotopic part of the material model is not achieved after sufficient accumulation of plastic strain. At low feed, this saturation has been reached and thus the feed has less influence.

The significant differences occur up to a depth of approximately 2.5 mm, an area that is highly plasticised with a deep-rolling force of 20 kN. The compensating area below this is no longer so strongly influenced by the accumulated plastic strain introduced, and the influence on the depth curve thus decreases. This is evident when looking in detail at the influence of the feed on the achieved depth effect, represented by the depth of the zero crossing. A slight decrease in the depth effect can be observed in both stress directions. Maximum tensile stresses exhibit opposite behaviour in

the circumferential and longitudinal directions. Although stresses in the circumferential direction increase with a higher feed rate, they decrease in the longitudinal direction.

The feed rate has an impact on the process application time and thus directly on the process costs, but it must be concluded that with the tool geometry considered and deep-rolling parameters, a feed rate of at least 0.5 mm should be realised to achieve a uniform residual stress state.

3.3 Friction coefficient

Figure 13 shows the influence of the friction coefficient between the tools and the workpiece on the residual stress depth profile. The large influence of the friction coefficient that is often assumed can be disproven, as already shown in [43]. It is concluded that considering a friction coefficient in the simulation is important, but that the level reached by this is of minimal influence. The reason for this is that the tool can be seen as a free-rolling wheel. The model does not consider rotational resistance. A good approximation to reality. Only resistances such as bearing friction occur here. These are very small and are therefore neglectable in the simulation. In the circumferential and longitudinal directions, however, very small differences are recognisable, marginally higher in the longitudinal direction than in the circumferential direction. The differences can be discussed by looking at the contact areas in detail. The tools are curved in two directions: in the longitudinal direction with the tool diameter and in the circumferential direction with the contact radius. In both directions, the material is compressed in front of the tools, then comes into contact and is pulled behind them. In contact formation in this region of the contact area, the coefficient of friction has a slight influence in both directions.

The modest impact on the residual stress in-depth curves is shown in Fig. 14 in the representation of the characteristic values of the residual stress depth curves as a function of the friction coefficient. The maximum compressive and tensile residual stresses are not influenced by the coefficient of

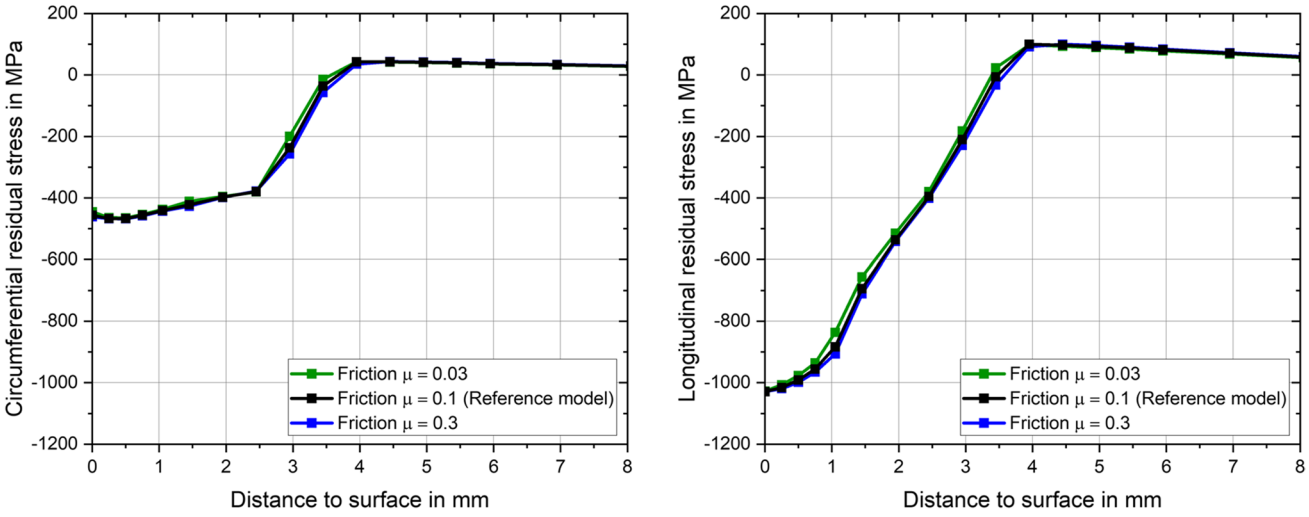

Fig. 13 Influence of the friction coefficient on the residual stresses in the circumferential (left) and longitudinal (right) directions

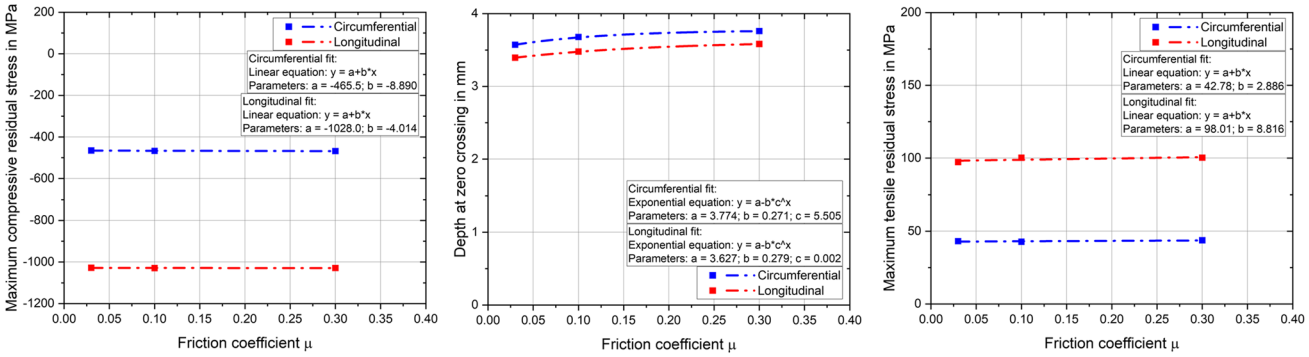

Fig. 14 Evaluation of the significant residual stress in-depth parameters versus friction coefficient

friction. It has a slight effect on the depth of the zero crossing. A lower coefficient of friction leads to a slightly lower effective depth, and a higher coefficient of friction leads to a slightly deeper achieved depth of zero crossing.

3.4 Number of overruns

The influence of the number of overruns is shown in Fig. 15 in circumferential (left) and longitudinal (right) directions. The first deep-rolling run has the greatest influence on the residual stresses. The second and third overruns show a very small influence on the introduced residual stress depth profile.

The small effect of the number of overruns is also evident in the evaluation of the characteristics of the residual stress depth profile, visible in Fig. 16. The most noticeable influence is seen in the maximum tensile residual stresses that occur. These reduce with repeated process application, whereby this influence also shows a tendency to decrease with an increasing number of overruns. The influence of repeated process applications is strongly material-dependent. The material used in this study shows a strong change in material properties with low applied strain but then stabilises quickly at a constant level with higher plastic strains occurring and no further changes shown. This behaviour is responsible for the barely changing residual stress state with repeated deep rolling. Although plastic deformations continue to be introduced more and more, they have minimal influence on the resulting residual stresses. The maximum residual compressive stresses and the depth of zero crossing remain nearly identical.

3.5 Deep-rolling tool geometry

In the following subsections, the geometry of the deep-rolling tool on the resulting residual stress in-depth curve is investigated. The geometry of the tool is changed by two parameters. These are, as already mentioned in Section 2.2.5, the diameter of the tool and the contact radius. The change in the two parameters influences the depth of

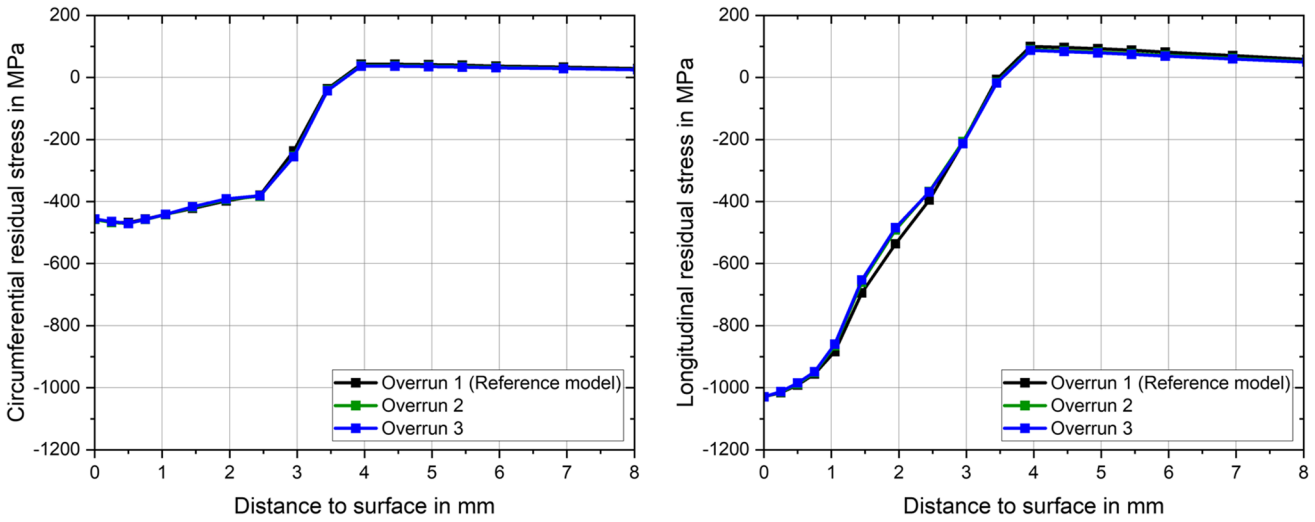

Fig. 15 Influence of the number of overruns on residual stresses in the circumferential (left) and longitudinal (right) directions

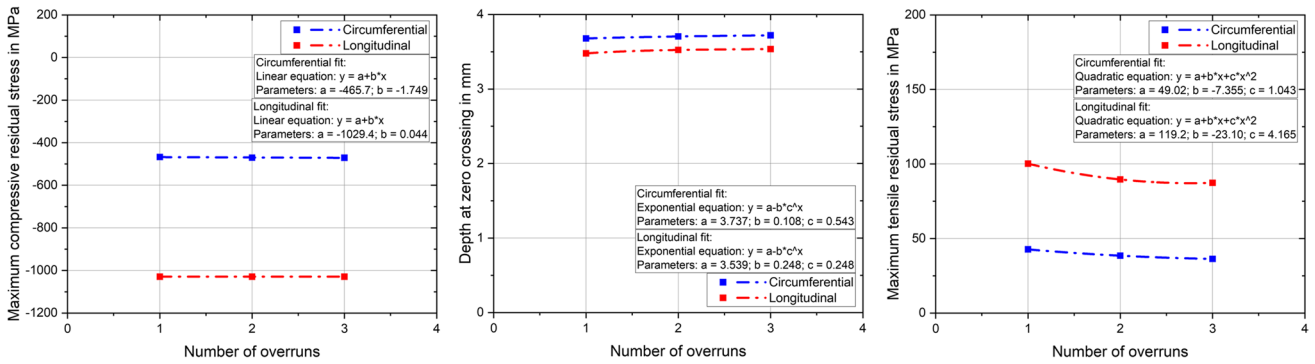

Fig. 16 Evaluation of the significant residual stress in-depth parameters versus the number of overruns

the contact area and the penetration between the tools and the workpiece.

3.5.1 Diameter

Figure 17 shows the influence of the diameter of the disc tool on the residual stress in-depth profile. Differences can be seen in both the circumferential and longitudinal directions.

The diameter of the tool influences the resulting contact area. When the deep-rolling force is applied, the contact surface is adjusted in such a way that a force equilibrium is achieved between the tool and the simulation model. Figure 18 shows the influence of the diameter of the tool on the resulting contact area. The larger tool diameter of 150 mm, compared to the reference diameter of 100 mm, results in a longer and thinner contact area. By contrast, a smaller diameter of 50 mm leads to a significantly shorter and broader contact patch.

Figure 19 shows the evaluation of the significant characteristic residual stress depth parameters over the tool

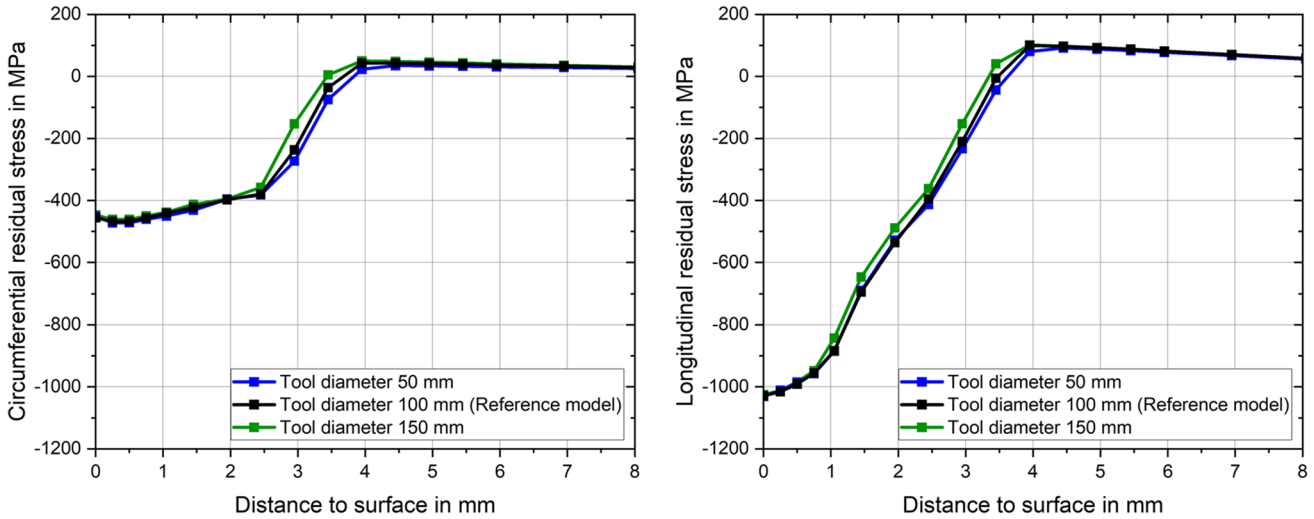

Fig. 17 Influence of the deep-rolling tool diameter on the residual stresses in the circumferential (left) and longitudinal (right) directions

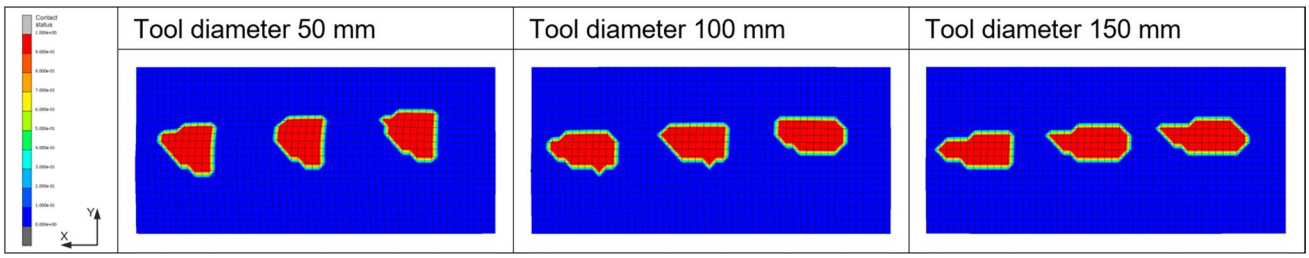

Fig. 18 Influence of tool diameter on the resulting contact status

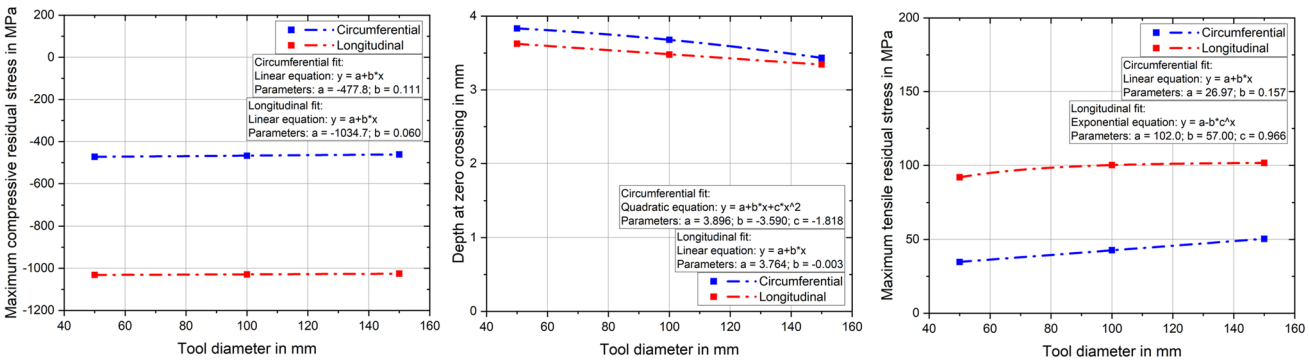

Fig. 19 Evaluation of the significant residual stress in-depth parameters versus tool diameter

diameter. Although the diameter has almost no influence on maximum compressive residual stresses, it does have an influence on the depth of zero crossing and on the maximum tensile residual stresses. Due to the strong plasticising and saturated state in the area near the surface, the tool diameter has virtually no influence on the present residual stress state. The changed contact surface also leads, in addition to the length and width of the contact area, to a changed penetration depth of the tool. Due to the different curvatures in the contact of the tool (diameter and contact radius), the tool sinks deeper with a smaller diameter and less deep with a larger diameter. This phenomenon can be used to explain the influence of the tool diameter on the depth of the zero crossing. A smaller diameter leads to a greater depth effect, and vice versa. The maximum tensile residual stresses increase slightly with a larger tool diameter.

3.5.2 Contact radius

The contact radius of the deep-rolling tool shows a slight influence on the residual stress depth curve rather than the diameter of the tool, visible in Fig. 20.

To understand the influence of the contact radius on residual stresses, the changed contact area must be observed again (Fig. 21). A smaller contact radius of 5 mm leads to a longer and thinner contact area compared to the reference contact radius of 9 mm, similar to the larger tool diameter. The larger contact radius leads to a shorter and wider contact area. The influence of the contact radius and the diameter on the contact area are in opposition to each other.

This opposite behaviour is also confirmed by evaluating the residual stress depth curves and the characteristic residual stress parameters, shown in Fig. 22. The negligible influence on the maximum compressive residual stresses is

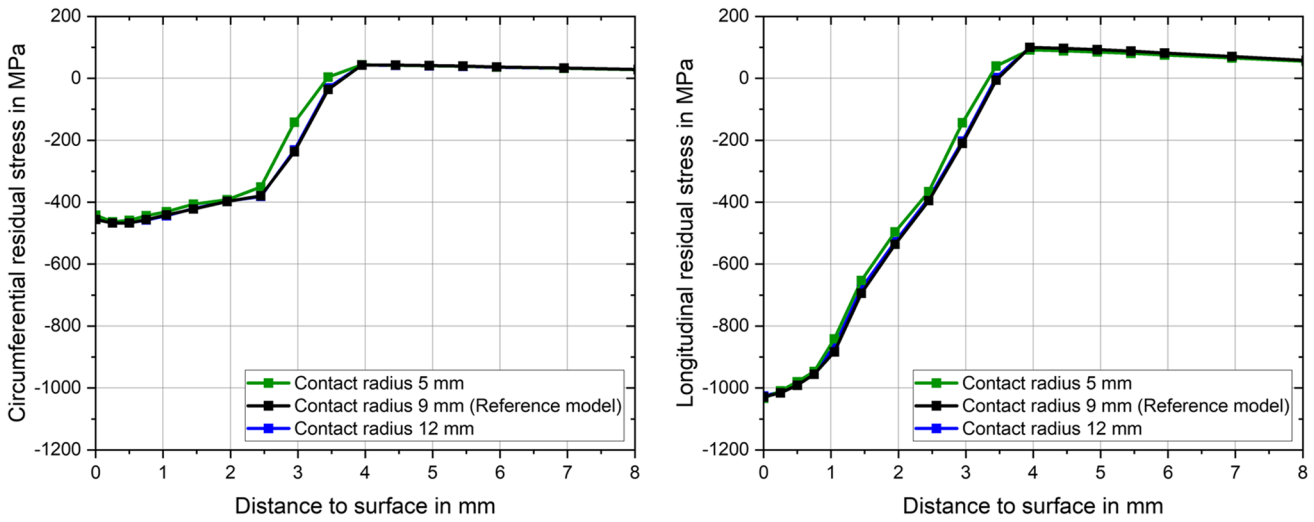

Fig. 20 Influence of the deep-rolling tool contact radius on the residual stresses in the circumferential (left) and longitudinal (right) directions

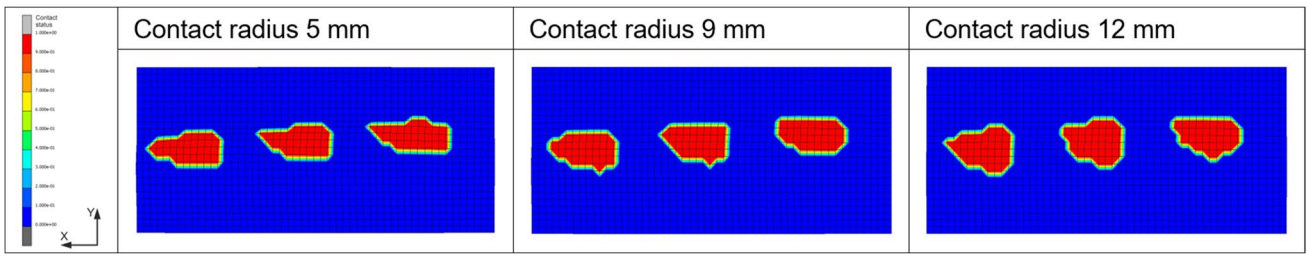

Fig. 21 Influence of the contact radius on the resulting contact status

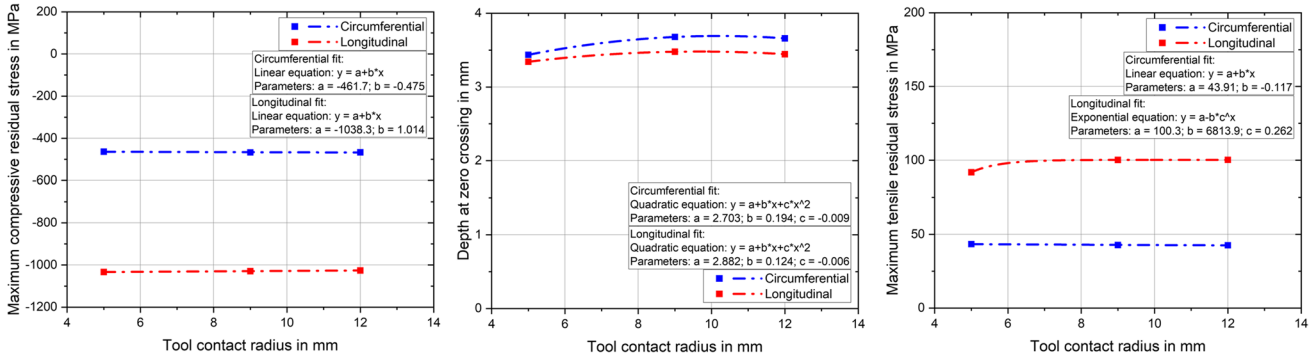

Fig. 22 Evaluation of the significant residual stress in-depth parameters versus tool contact radius

also confirmed for different contact radii. The depth of the zero crossing shows a dependence on the contact radius. The influence of the contact area and the resulting sinking depth are found to be the same as for the tool diameter. A smaller contact radius, thus longer and narrower contact and less penetration depth, also leads to a smaller depth effect on the residual stresses. The opposite behaviour occurs with a larger contact radius, whereby the absolute influence decreases significantly. The maximum occurring tensile residual stresses tend to increase slightly with increasing contact radius.

3.6 Railway axle diameter

The influence of the railway axle diameter on the introduced residual stresses is examined using simulation models with the adapted outer shaft contour presented in Section 2.2.6. Figure 23 shows the influence of different shaft diameters on the resulting in-depth residual stress distribution. It is immediately apparent that this mainly influences the stresses' circumferential direction.

The adjusted geometry of the simulation model has an effect on the resulting contact area between the axle surface and the tools, visible in Fig. 24. A smaller shaft diameter leads to a shorter and wider contact, and vice versa, a larger diameter leads to a longer and narrower contact zone.

The shorter contact length results again in an enhanced depth effect, as with the change in tool geometry, although in this case, it is comparably small, as can be seen in Fig. 23. More influence can be seen in the compressive and tensile residual stress regions, especially in the circumferential direction, where the change in the geometry of the shaft contour has its main effect. Untypical behaviour is evident. Although lower compressive residual stresses occur, the compensating tensile residual stresses are not reduced but reveal a higher magnitude. This phenomenon is most likely due to the stiffening geometry of the shaft contour. The results show consistent behaviour. The smallest diameter

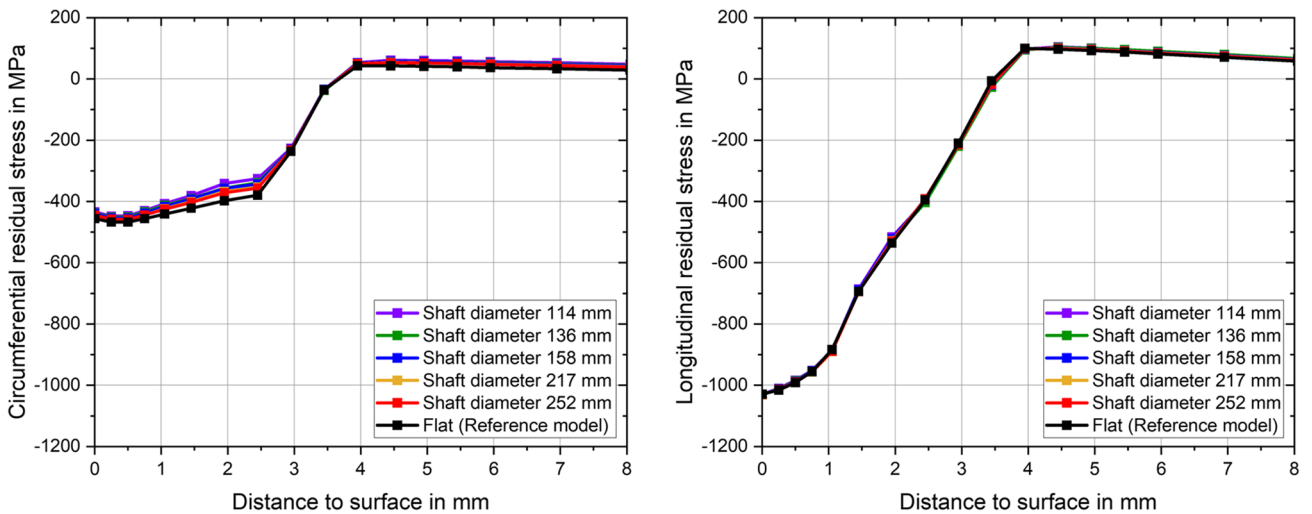

Fig. 23 Influence of the shaft diameter on the residual stresses in the circumferential (left) and longitudinal (right) directions

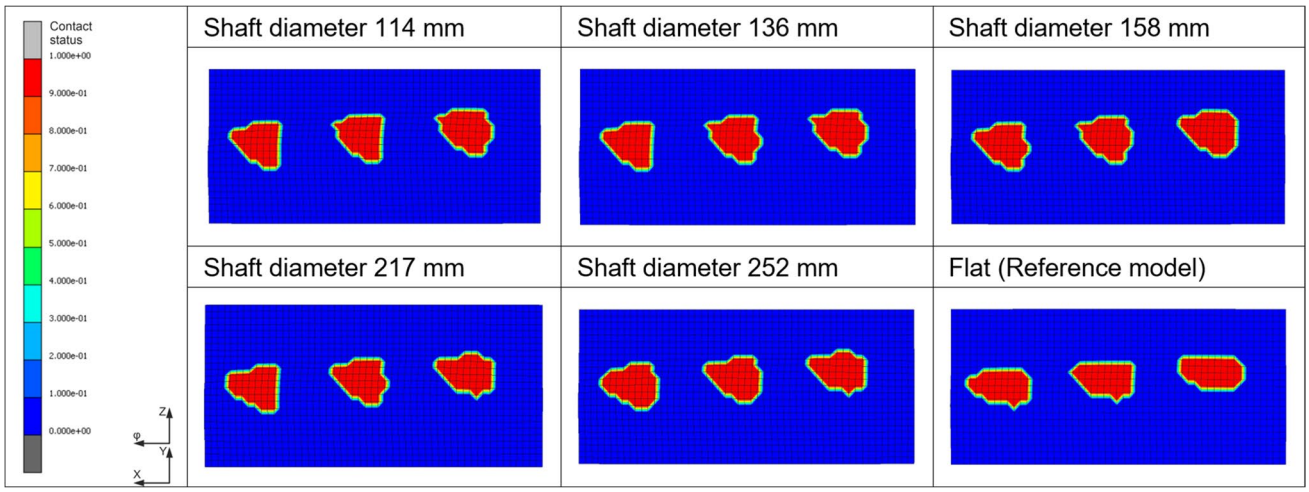

Fig. 24 Influence of the shaft geometry on the resulting contact status

results in the lowest compressive residual stresses and the highest tensile residual stresses in the circumferential direction. Larger compressive residual stresses and lower tensile residual stresses are introduced in the circumferential direction with increasing diameter, thus decreasing surface curvature towards the flat reference model.

The evaluation of the characteristic parameters of the residual stress in-depth profiles over the shaft diameter is shown in Fig. 25. In addition to the evaluations of the simulation models with shaft geometry, the result of the flat simulation model is shown. The difference in the circumferential direction, which is clearly visible in Fig. 23, is almost invisible in the evaluations in Fig. 25. The differences occur between the maximum compressive residual stresses and the zero crossing and are therefore not recorded. The maximum compressive residual stresses show almost no dependence on the shaft diameter. The depth of zero crossing and the maximum tensile residual stresses decrease slightly with increasing shaft diameter.

3.7 Process applicability and optimisation

As already mentioned, a direct recommendation regarding the best choice of parameters is difficult just on the basis of the residual stresses applied and requires further evaluations of the results. Nevertheless, the applicability of the results is subsequently summarised only considering the introduced residual stresses and their influence on the characteristic residual stress parameters. The aim of the treatment is to achieve compressive residual stresses near the surface, the most pronounced depth effect possible, and the lowest possible balancing tensile residual stresses.

The deep-rolling force has the most significant influence on the residual stress state introduced. The maximum compressive residual stresses occur at or near the surface, increase with increasing deep-rolling force, and reach a maximum at approximately – 1000 MPa, which is limited by the material properties. The depth effect in particular can be significantly elevated with increased forces, but the

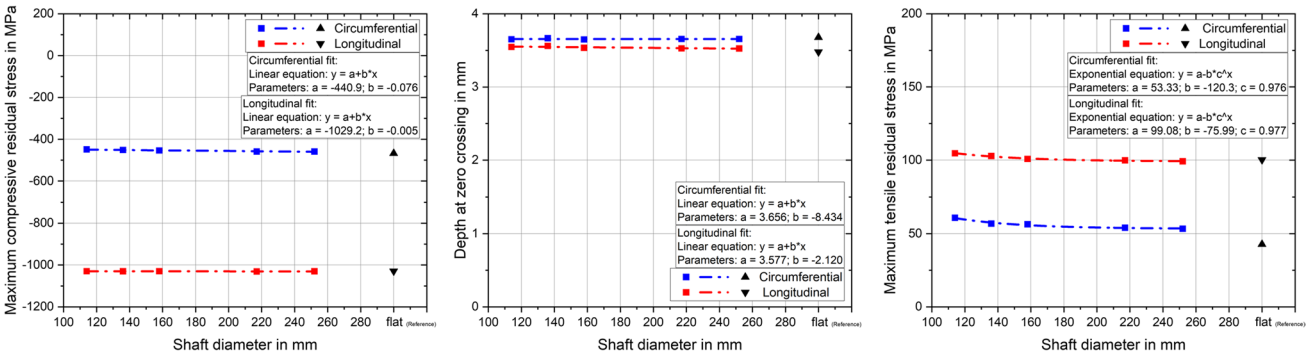

Fig. 25 Evaluation of significant residual stress in-depth parameters versus shaft diameter

compensating tensile residual stresses also increase with increasing deep-rolling force, which may lead to decreased fatigue strength. High deep-rolling forces are recommended if deeper compressive residual stress states are desired, but due to the increased plasticising of the material in the near-surface region and the associated damage, the applicable deep-rolling force increase is limited.

The feed rate shows an influence on the residual stresses introduced. High feed rates lead to uneven residual stress conditions and should therefore be avoided, even if the machining time is reduced. A feed rate of at least 0.5 mm is recommended for the prevailing boundary conditions. The friction coefficient and also the number of overruns with the same deep-rolling forces show a minor influence on the introduced residual stresses, so no benefit can be found in a changed application. The geometry of the tool is certainly related to the deep-rolling tools available on the market. However, a smaller tool diameter and larger contact radius tend to result in a greater depth effect and therefore show a positive influence on the residual stresses introduced. The diameter of the railway axle is not a parameter that can be changed; it is determined by the axle to be machined. Anyway, the influence of the railway axle diameter on the introduced residual stresses is comparably low. A minor influence can be observed in the circumferential direction, while in the longitudinal direction, the residual stress profiles are almost identical.

Multiple deep rolling with decreasing deep-rolling forces show optimised effects on the introduced residual stresses. In Fig. 26, the influence of this optimisation on the residual stress depth profiles is shown. The result of the simulation deep rolled with reference parameters is compared with the results of repeated deep rolling with 20 kN and followed by 10 kN (20 kN/10 kN), with 20 kN and followed by 5 kN (20 kN/5 kN) and with 20 kN, followed by 10 kN and finally 5 kN (20 kN/10 kN/5 kN).

Remarkably, the last processing step determines the residual stresses in the area close to the surface, the area with strong plasticising, below which the residual stress states approach the before-prevailing state. This phenomenon is particularly evident for the stresses in the longitudinal direction. The additional machining with 10 or 5 kN causes the residual stress state similar to the single machining with the respective force up to a depth of approximately 1.5 or 1.0 mm, followed by a transition to the residual stress state accused by the previous treatment with 20 kN. Machining with three consecutive passes, the residual stress state is dominant from machining with 5 kN to a depth of approximately 1 mm, followed by the state triggered by machining with 10 kN, and then the residual stress state with 20 kN.

The influence of the optimisations on the characteristic residual stress parameters is shown in Fig. 27. As the "degree of optimisation" increases, there is a decreasing trend in the maximum compressive residual stresses. The decrease is slight in the circumferential direction and more pronounced in the longitudinal direction, but compressive residual stresses of – 800 MPa are still present. The depth of the zero crossing increases with repeated machining; the effect is more significant in the longitudinal direction. The effect of multiple deep rolling with decreasing forces on the compensating tensile residual stresses is particularly beneficial. A significant reduction is again evident in the longitudinal direction. Compared to machining with reference parameters, the residual tensile stresses can be reduced by more than half.

In summary, optimisation with repeated deep rolling with decreasing deep-rolling force can increase the depth

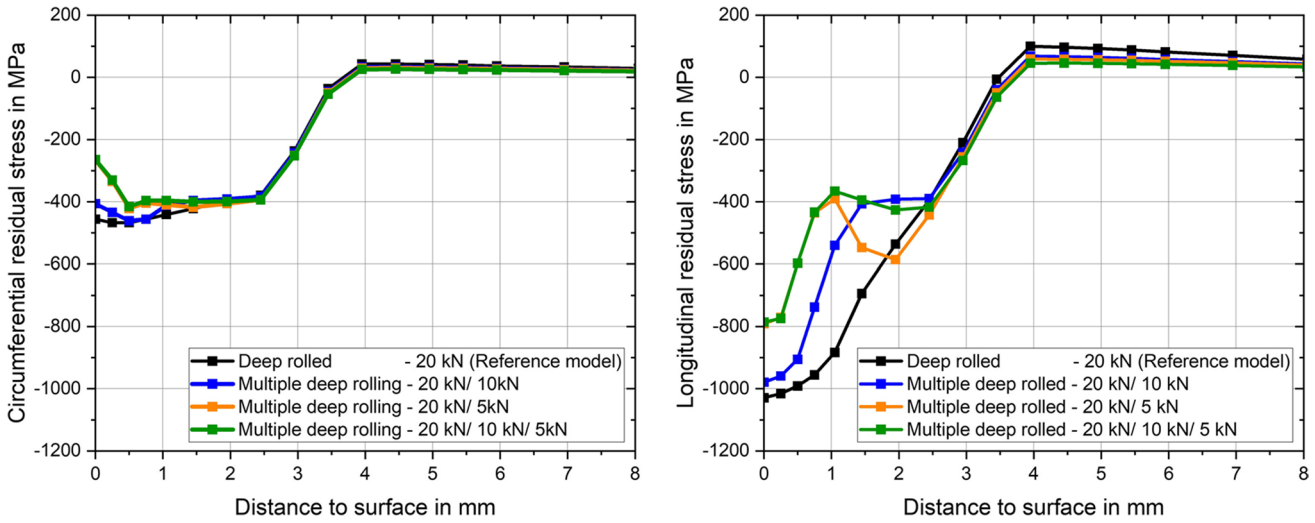

Fig. 26 Influence of the optimisation with multiple deep rolling with decreasing deep-rolling forces on the residual stresses in the circumferential (left) and longitudinal (right) directions

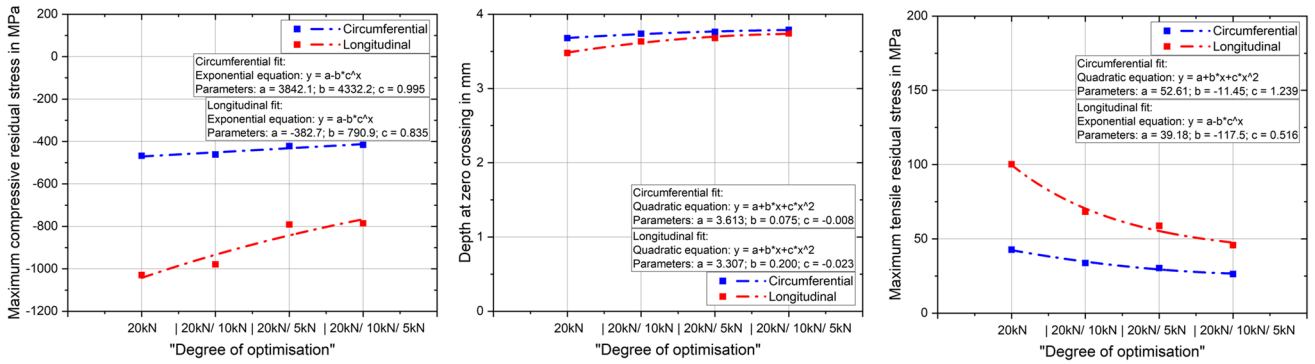

Fig. 27 Evaluation of significant residual stress in-depth parameters versus the "degree of optimisation" with multiple deep rolling with decreasing deep-rolling forces

effect and significantly reduce the tensile residual stresses by reducing the compressive residual stress zone. The compressive residual stress level is still very high.

4 Summary and conclusions

Within the scope of this study, the influence of main deep-rolling process parameters on the residual stress in-depth distribution is numerically investigated. A validated simulation model is used as a basis, which was defined as a reference model. Within the framework of the parameter variation, only one parameter is changed at a time, and the influence of the one parameter is explicitly analysed. The influence of the deep-rolling force, feed rate, friction coefficient, number of overruns, tool geometry, and different shaft diameters are investigated. Furthermore, a deep-rolling optimisation proposal with multiple deep rolling with decreasing deep-rolling forces is presented. The results can be summarised in the following points regarding the influence of the individual parameters investigated:

- The deep-rolling force has the greatest impact on the residual stresses. The maximum compressive residual stresses that occur increase with a higher deep-rolling force and reach saturation with an applied force of 10 kN at around − 1000 MPa. The deep-rolling force has a huge effect on the achieved effective depth of the process and shifts the transition from compressive to compensatory tensile residual stresses further into the depth. A wide range occurs; a deep-rolling force of 2 kN causes a zero crossing at a depth of 1 mm and a force of 20 kN at 3.5 mm. The compensating tensile residual stresses increase with increasing deep-rolling force and also show saturation behaviour at + 100 MPa.
- Low feed rates with values of 0.25 and 0.5 mm show minimal influence on the simulation results, and the residual stress in-depth curves are almost congruent. The repeated contact of the tools at the same point in the simulation model and the thus achieved saturation effect of the used material behaviour can be stated as the reason for this behaviour. Higher feed rates lead to a reduction of the compressive residual stresses from more than − 1000 to − 900 MPa near the surface and a slightly reduced effective depth. Machining time can be reduced with higher feed rates, but if the feed rate chosen is too high, here 1.0 and 2.0 mm, an undesired non-uniform residual stress state is obtained. Therefore, a feed rate of at least 0.5 mm is recommended.
- The coefficient of friction has a minimal influence on the residual stress result due to the free-rolling tool. A tendency to lower the achieved depth effect with a lower coefficient of friction, and vice versa, can be stated. The influence on the maximum compressive and tensile residual stresses introduced can be neglected.
- The number of overruns has a minor effect only on the introduced residual stresses. The stress state applied by the first treatment remains similar by treating for the second and third times. The shown behaviour is again caused by the saturating effect of the material with accumulated strains. The introduced change in the remaining strains after multiple deep rolling therefore leads to a slightly modified residual stress state. A tendency to a larger depth of zero crossing and lower tensile residual stresses occurs with an increasing number of treatments.
- The influence of the tool geometry is investigated by changing the tool diameter and the contact radius of the used disc tools. Both changes in geometry influence the area of contact between the tool and the simulation model. The correlation found is that a smaller tool diameter and a larger contact radius lead to a shorter and wider contact area. This allows the tool to penetrate deeper, and as a result, a greater depth effect is achieved. By contrast, a larger diameter and smaller contact radius will lead to a longer and narrower contact surface and thus lowerdepth effect. The geometry

Table 2 Summary of the parameter sensitivity analysis. Parameter influence on the maximum compressive residual stresses, the achieved depth of zero crossing and the maximum tensile residual stresses

Increased … leads to	Maximum compressive residual stresses	Depth of zero crossing	Maximum tensile residual stresses
Deep-rolling force	↑↑↑	↑↑↑	↑↑↑
Feed rate	↓	↓↓	C. ↑↑ L. ↓↓
Friction coefficient	→	↑↑	→
Number of overruns	→	↑	↓↓
Tool diameter	→	↓↓	↑↑
Tool contact radius	→	↑↑	↑
Railway axle diameter	→	→	↓↓
"Degree of optimisation"	↓	↑↑	↓↓↓

"↑" small influence; "↑↑" medium influence; "↑↑↑" large influence; *C.* circumferential; *L.* longitudinal

of the tools shows negligible influence on the maximum residual compressive stresses and a minor effect on the maximum tensile residual stresses.

- The simulation model is adapted to the shaft geometry; different shaft diameters are considered, and the results are compared. Differences from the flat simulation model are evident in the residual stress in-depth profiles in the circumferential direction. There are slightly less compressive residual stresses and slightly increased tensile residual stresses. The diameter of the shaft has negligible influence on the maximum compressive residual stresses and the depth of zero crossing. The maximum tensile residual stresses decrease slightly with increasing diameter.
- The optimisation with multiple deep-rolling treatments with decreasing forces shows a positive effect on the introduced residual stress state. The most promising result is achieved with treatment with 20 kN, followed by deep rolling with 10 kN, and finally with 5 kN. The compressive residual stress amount is slightly reduced but still remains at a high level. The depth effect is increased and the undesirable balancing tensile residual stresses are significantly reduced.

In Table 2, the influence of the investigated parameters on the characteristic points of the residual stress in-depth profile is summarised. The individual columns contain the investigated deep-rolling parameters, and the arrows indicate the influence of an increase of the respective parameter on the characteristic points. An arrow pointing upwards indicates an increase, and an arrow pointing downwards indicates a decrease in the level of the characteristic points. The number of arrows indicates the magnitude of the influence of the parameter. One arrow means small influence, two arrows mean medium influence, and three arrows mean large influence. If the circumferential and longitudinal results show inverse results, a remark to the stress direction is added; otherwise, the effect is similarly evaluated in both directions.

The presented work shows the influence of various deep-rolling parameters on the introduced residual stress state by using a validated simulation model. The obtained information provides the foundation for optimising the residual stress depth profile and can be used to optimise the lifetime of railway axles. Important properties such as service life, lightweight construction to reduce the unsprung masses, and economic efficiency of railway axles can be increased [48]. The deep-rolling process and the associated increase in service life are strongly dependent on the material. The presented investigation is valid for the high-strength steel 34CrNiMo6; for other materials, a corresponding material model must be developed and can be added to the simulation model. The process can be further optimised with regard to the component lifetime, and wheelset-specific investigations can be examined numerically.

Funding Open access funding provided by Graz University of Technology.

Declarations

Competing interests The authors declare no competing interests.

References

1. Rieger M et al (2020) Fatigue crack growth in full-scale railway axles – influence of secondary stresses and load sequence effects. Int J Fatigue 132:105360. https://doi.org/10.1016/j.ijfatigue.2019.105360
2. Simunek D, Leitner M, Maierhofer J, Gänser H-P, Pippan R (2019) Analytical and numerical crack growth analysis of 1:3 scaled railway axle specimens. Metals 9(2):184. https://doi.org/10.3390/met9020184
3. Mahmoudi AH, Ghasemi A, Farrahi GH, Sherafatnia K (2016) A comprehensive experimental and numerical study on redistribution of residual stresses by shot peening. Mater Des 90:478–487. https://doi.org/10.1016/j.matdes.2015.10.162
4. Starker P, Macherauch E (1983) Kugelstrahlen und Schwingfestigkeit. Mat.-wiss. u. Werkstofftech. 14:109–115. https://doi.org/10.1002/mawe.19830140406
5. Balland P, Tabourot L, Degre F, Moreau V (2013) An investigation of the mechanics of roller burnishing through finite element simulation and experiments. Int J Mach Tools Manuf 65:29–36. https://doi.org/10.1016/j.ijmachtools.2012.09.002
6. John MS, Wilson AW, Bhardwaj AP, Abraham A, Vinayagam BK (2016) An investigation of ball burnishing process on CNC lathe using finite element analysis. Simul Model Pract Theory 62:88–101. https://doi.org/10.1016/j.simpat.2016.01.004
7. Delgado P, Cuesta II, Alegre JM, Díaz A (2016) State of the art of deep rolling. Precis Eng 46:1–10. https://doi.org/10.1016/j.precisioneng.2016.05.001
8. Röttger K, Wilcke G, Mader S (2005) Festwalzen - eine Technologie für effizienten Leichtbau. Mat-wiss u Werkstofftech 36(6):270–274. https://doi.org/10.1002/mawe.200500876
9. Leitner M, Simunek D, Shah SF, Stoschka M (2018) Numerical fatigue assessment of welded and HFMI-treated joints by notch stress/strain and fracture mechanical approaches. Adv Eng Softw 120:96–106. https://doi.org/10.1016/j.advengsoft.2016.01.022
10. Foehrenbach J, Hardenacke V, Farajian M (2016) High frequency mechanical impact treatment (HFMI) for the fatigue improvement: numerical and experimental investigations to describe the condition in the surface layer. Weld World 60(4):749–755. https://doi.org/10.1007/s40194-016-0338-4
11. Hassani-Gangaraj SM, Carboni M, Guagliano M (2015) Finite element approach toward an advanced understanding of deep rolling induced residual stresses, and an application to railway axles. Mater Des 83:689–703. https://doi.org/10.1016/j.matdes.2015.06.026
12. Schulze V (2006) Modern mechanical surface treatment: States, stability, effects. Zugl.: Karlsruhe, Univ., Habil.-Schr., 2004. Wiley-VCH, Weinheim
13. Altenberger I (2005) Deep rolling - the past, the present and the future, University of Kassel, Institute of Materials Engineering, Monchebergstrasse 3, 34125 Kassel. Germany 2005:144–155
14. Berstein G, Fuchsbauer B (1982) Festwalzen und Schwingfestigkeit. Z Werkstofftechnik 1982(13):103–109
15. Beghini M, Bertini L, Monelli BD, Santus C, Bandini M (2014) Experimental parameter sensitivity analysis of residual stresses induced by deep rolling on 7075–T6 aluminium alloy. Surf Coat Technol 254:175–186. https://doi.org/10.1016/j.surfcoat.2014.06.008
16. Schubnell J, Farajian M (2022) Fatigue improvement of aluminium welds by means of deep rolling and diamond burnishing. Weld World 66(4):699–708. https://doi.org/10.1007/s40194-021-01212-1
17. Hadadian A (2019) Finite element analysis and design optimization of deep cold rolling of titanium alloy at room and elevated temperatures. PhD Thesis, Department of Mechanical, Industrial and Aerospace Engineering, Concordia University, Montreal, Quebec, Canada
18. Huang J et al (2019) Effect of thermal annealing on the microstructure, mechanical properties and residual stress relaxation of pure titanium after deep rolling treatment. J Mater Sci Technol 35(3):409–417. https://doi.org/10.1016/j.jmst.2018.10.003
19. Uddin M, Hall C, Hooper R, Charrault E, Murphy P, Santos V (2018) Finite element analysis of surface integrity in deep ball-burnishing of a biodegradable AZ31B Mg alloy. Metals 8(2):136. https://doi.org/10.3390/met8020136
20. Gharbi K, Ben Moussa N, Ben Rhouma A, Ben Fredj N (2021) Improvement of the corrosion behavior of AISI 304L stainless steel by deep rolling treatment under cryogenic cooling. Int J Adv Manuf Technol 117:3841–3857. https://doi.org/10.1007/s00170-021-07744-6
21. Muñoz-Cubillos J, Coronado JJ, Rodríguez SA (2017) Deep rolling effect on fatigue behavior of austenitic stainless steels. Int J Fatigue 95:120–131. https://doi.org/10.1016/j.ijfatigue.2016.10.008
22. Abrão AM, Denkena B, Köhler J, Breidenstein B, Mörke T (2014) The influence of deep rolling on the surface integrity of AISI 1060 high carbon steel. Procedia CIRP 13:31–36. https://doi.org/10.1016/j.procir.2014.04.006
23. Perenda J, Trajkovski J, Žerovnik A, Prebil I (2015) Residual stresses after deep rolling of a torsion bar made from high strength steel. J Mater Process Technol 218:89–98. https://doi.org/10.1016/j.jmatprotec.2014.11.042
24. Perenda J, Trajkovski J, Žerovnik A, Prebil I (2016) Modeling and experimental validation of the surface residual stresses induced by deep rolling and presetting of a torsion bar. Int J Mater Form 9(4):435–448. https://doi.org/10.1007/s12289-015-1230-2
25. European Standard. EN 13261: Railway applications - Wheelsets and bogies - Axles - Product requirements. EN 13261 2021
26. Linhart V, Černý I (2011) An effect of strength of railway axle steels on fatigue resistance under press fit. Eng Fract Mech 78(5):731–741. https://doi.org/10.1016/j.engfracmech.2010.11.023
27. Novosad M, Fajkoš R, Řeha B, Řezníček R (2010) Fatigue tests of railway axles. Procedia Eng 2(1):2259–2268. https://doi.org/10.1016/j.proeng.2010.03.242
28. Thöni C (2014) Auslegung und Planung eines Prüfstandes zur Erzeugung einer umlaufenden Biegespannung an Radsatzwellen. Diplomarbeit, Institut für Leichtbau, Technische Universität Graz, Graz
29. Ecoroll AG. www.ecoroll.de
30. Hadadian A, Sedaghati R (2019) Investigation on thermal relaxation of residual stresses induced in deep cold rolling of Ti–6Al–4V alloy. Int J Adv Manuf Technol 100(1–4):877–893. https://doi.org/10.1007/s00170-018-2668-4
31. Forschungskuratorium Maschinenbau (FKM) (2020) FKM-Richtlinie: Rechnerischer Festigkeitsnachweis für Maschinenbauteile: aus Stahl, Eisenguss- und Aluminiumwerkstoffen. FKM-Richtlinie
32. Deutsche Norm. DIN 743–2: Tragfähigkeitsberechnung von Wellen und Achsen: Teil 2: Formzahlen und Kerbwirkungszahlen. DIN 743–2 2012
33. Pertoll T et al (2023) Experimental and numerical investigation of the deep rolling process focussing on 34CrNiMo6 railway axles. Int J Mater Form 16(5). https://doi.org/10.1007/s12289-023-01775-y
34. Sartkulvanich P, Altan T, Jasso F, Rodriguez C (2007) Finite element modeling of hard roller burnishing: an analysis on the effects of process parameters upon surface finish and residual stresses. J

Manuf Sci Eng 129(4):705–716. https://doi.org/10.1115/1.2738121
35. Lyubenova N, Baehre D (2015) Finite element modelling and investigation of the process parameters in deep rolling of AISI 4140 Steel. JMSE-B 5(8). https://doi.org/10.17265/2161-6221/2015.7-8.004
36. Alshareef AJ, Marinescu ID, Basudan IM, Alqahtani BM, Tharwan MY (2020) Ball-burnishing factors affecting residual stress of AISI 8620 steel. Int J Adv Manuf Technol 107(3–4):1387–1397. https://doi.org/10.1007/s00170-020-05119-x
37. El-Axir MH (2000) An investigation into roller burnishing. Int J Mach Tools Manuf 40(11):1603–1617. https://doi.org/10.1016/S0890-6955(00)00019-5
38. Rami A, Gharbi F, Sghaier S, Hamdi H (2018) Some insights on combined turning-burnishing (CoTuB) process on workpiece surface integrity. Int J Precis Eng Manuf 19(1):67–78. https://doi.org/10.1007/s12541-018-0008-0
39 Majzoobi GH, TeimoorialMotlagh S, Amiri A (2010) Numerical simulation of residual stress induced by roll-peening. Trans Indian Inst Met 63(2–3):499–504. https://doi.org/10.1007/s12666-010-0071-4
40 Bäcker V, Klocke F, Wegner H, Timmer A, Grzhibovskis R, Rjasanow S (2010) Analysis of the deep rolling process on turbine blades using the FEM/BEM-coupling. IOP Conf Ser: Mater Sci Eng 10:12134. https://doi.org/10.1088/1757-899X/10/1/012134
41. Klocke F, Bäcker V, Wegner H, Zimmermann M (2011) Finite element analysis of the roller burnishing process for fatigue resistance increase of engine components. Proc Inst Mech Eng Part B: J Eng Manuf 225(1):2–11. https://doi.org/10.1243/09544054JEM2044
42. Han K, Zhang D, Yao C, Tan L, Zhou Z, Zhao Y (2021) Investigation of residual stress distribution induced during deep rolling of Ti-6Al-4V alloy. Proc Inst Mech Eng Part B: J Eng Manuf 235(1–2):186–197. https://doi.org/10.1177/0954405420947960
43. Lim A, Castagne S, Wong CC (2016) Effect of deep cold rolling on residual stress distributions between the treated and untreated regions on Ti–6Al–4V alloy. J Manuf Sci Eng 138(11). https://doi.org/10.1115/1.4033524
44. Manouchehrifar A, Alasvand K (2012) Finite element simulation of deep rolling and evaluate the influence of parameters on residual stress. Recent Researches in Applied Mechanics
45. Mohammadi F, Sedaghati R, Bonakdar A (2014) Finite element analysis and design optimization of low plasticity burnishing process. Int J Adv Manuf Technol 70(5–8):1337–1354. https://doi.org/10.1007/s00170-013-5406-y
46. Sayahi M, Sghaier S, Belhadjsalah H (2013) Finite element analysis of ball burnishing process: comparisons between numerical results and experiments. Int J Adv Manuf Technol 67(5–8):1665–1673. https://doi.org/10.1007/s00170-012-4599-9
47. Mombeini D, Atrian A (2018) Experimental and numerical investigation of the effects of deep cold rolling on the bending fatigue tolerance of C38500 brass alloy. Int J Adv Manuf Technol 97(5–8):3039–3053. https://doi.org/10.1007/s00170-018-2165-9
48. Marschnig S (2016) Innovative track access charges. Transp Res Procedia 14:1884–1893. https://doi.org/10.1016/j.trpro.2016.05.155